Monte Carlo Simulation of Terahertz Quantum-Cascade Lasers

H. Li and J. C. Cao *
State Key Laboratory of Functional Materials for Informatics,
Shanghai Institute of Microsystem and Information Technology,
Chinese Academy of Sciences,
865 Changning Road, Shanghai 200050, China
* Email: jccao@mail.sim.ac.cn

Abstract: An ensemble Monte Carlo model is used to evaluate the bias and temperature dependent performance of a 4.1-THz quantum cascade laser with four-well resonant-phonon design. Carrier transport and gain characteristics are investigated. A buleshift in lasing frequency with increasing temperature is clearly observed. Because the broadening effect of temperature dependent gain profile is excluded in the model, our calculations overestimate the peak gain and subsequently overrate the maximum operating temperature. Under a linear approximation condition, the deduced maximum operating temperature is in good agreement with experiment. The simulation also shows that the lasing frequency is insensitive to temperature.

Key words: terahertz, quantum cascade laser, Monte Carlo

doi: 10.11906/TST.230-236.2008.12.19

1. Introduction

Terahertz (THz) radiation source is the key device in the application of THz technology. As a compact and coherent source, THz quantum cascade laser (QCL) in which the optical transition can be tailored by engineering the multiple-quantum-well active layer attracts much interests from researchers. Since the first demonstration of THz QCLs, significant improvements have been made over the past few years [1,2]. Up to now, the available lowest lasing frequency is 1.2 THz without the assistance of a magnetic field [3], the highest operating temperature is 178 K in pulsed mode [4] and 117 K in continuous-wave (cw) mode [5], and the highest light power is 248 mW [6]. Further performance improvement will lead to wider applications. So the pursue of higher output power, higher working temperature, and wider lasing frequency never stops.

In this article, we use an ensemble Monte Carlo (MC) method [7] to evaluate the bias and temperature dependent performance of the non-equilibrium device. Carrier transport and gain characteristics are investigated.

2. Device structure and Monte Carlo Model

The device structure is based on a four-well resonant-phonon design and a double-metal waveguide. The active region of the THz QCL comprises 178 repeats of the cascaded period given in Fig. 1, where we show a calculated conduction-band profile together with the squared wave functions of the most important states under the design bias of 59 *mV*/module (11 *kV/cm*). As shown in Fig. 1, the THz phonon is generated from the radiation transition between upper lasing level 5 and lower lasing level 4, where the transition energy E_{54} and the oscillator strength f_{54} are calculated to be 17.5 *meV* (4.2 *THz*) and 0.68, respectively. Electron depopulation in level 4 is achieved by fast resonant longitudinal-optical (LO) phonon scattering into levels 1 and 2. The population inversion conditions, i.e., τ_5=4.43 *ps*, τ_4=0.42 *ps*, and τ_{54}=59 *ps*, are achieved at the design bias.

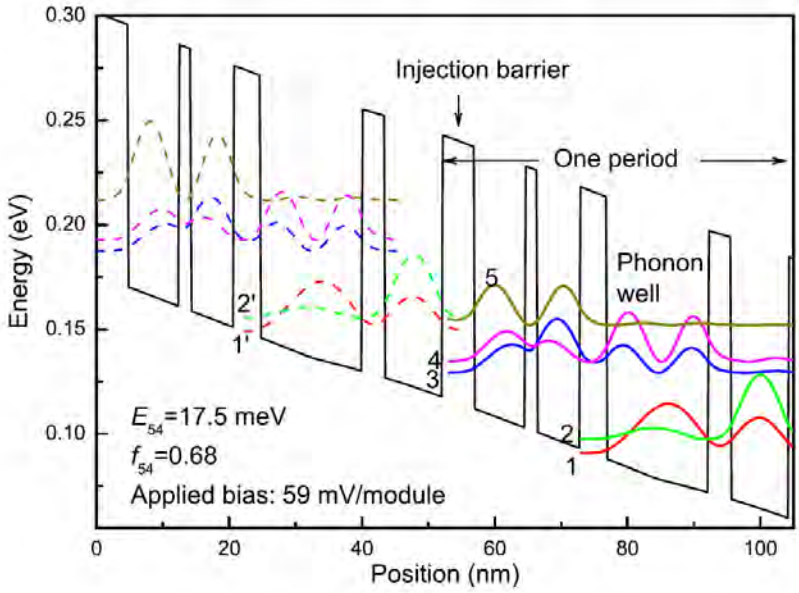

Fig. 1 Calculated conduction-band structure and squared wave functions of the most important states under the design bias of 11 kV/cm. From the left injection barrier, the layer thicknesses of the four-well module are **48.1**/79.1/**19.8**/65/**42.4**/158.3/**33.9**/90.5 in angstrom, where the $Al_{0.15}Ga_{0.85}As$ barriers are in boldface and GaAs wells in plain text. The center 36 Å of the underlined well is doped to 3.6×10^{10} cm^{-2} per module.

The QCL wafer was grown by molecular beam epitaxy (MBE) on a semi-conducting GaAs (100) substrate and fabricated into 40-μm-wide and 1-mm-long double metal waveguide structure using In-Au wafer bonding. An ensemble MC method, including electron-electron (e-e), electron-LO-phonon (e-p), electron-impurity (e-i) scatterings, and the hot-phonon effect [8], is used to evaluate the bias and temperature dependent performance of the THz QCL. The single subband static screening model and the periodic boundary conditions are applied in the MC model. To include the hot phonon effect in our MC model, the decay time constant of LO phonon τ_{LO} should be assumed. Many theoretical and experimental work have been carried out to determine the lifetime of LO phonon, which shows that τ_{LO} in bulk GaAs is between 3.5 to 10 *ps*. Actually, it is not easy to obtain a very precise value of LO phonon lifetime in GaAs-based THz QCLs; consequently, we use τ_{LO}=5 *ps* in our calculations. Details about the MC model are available in our previous work [8-11].

3. Results and discussion

Calculated carrier transport characteristics are shown by *I-V* curves in Fig. 2(a). The diamonds are the sampling points and the dashed line provides a guide to the eye. As a reference, the measured *I-V* curve is also indicated by a full line. The measured *I-V* curve is adjusted to account for a parasitic series resistance of 1 *Ω* and a parallel resistance of 150 *Ω* for fitting the simulated curve. We dunt a large parasitic current density at 7.4 *kV/cm*, where the electrons are injected from the injection state 1' into lower lasing state 4 directly without experiencing the radiative transition. The simulation agrees well with the measured result under the fitting conditions. Because of the large energy separation between the lasing states, the calculated parasitic current density (650 A/cm^2) is much smaller than that of other structures with lower lasing frequency [10]. Hence, we suggest that the parasitic current effect is more severe in the structure with lower emission frequency which should be one reason for the difficulty in achieving low-frequency THz QCLs. Figure 2(b) shows the gain characteristic of the device. The peak gain of 66 cm^{-1} is obtained at 11 *kV/cm*. To evaluate the threshold of the device, we also calculated the threshold gain g_{th} given by $g_{th}=(\alpha_M+\alpha_W)/\Gamma$, where α_M is the mirror loss, α_W is the waveguide loss, and Γ is the mode confinement factor. We use the facet reflectivity of 78% to calculate the mirror loss [13]. The Drude model, with relaxation time constants τ=0.1 *ps* and τ_{LO}=0.5 *ps* for heavily doped GaAs contact layers and lightly doped active region, respectively, is used to determine the waveguide loss. The gold refractive index is assumed to be 163+ i351 [14]. The one-dimensional calculation of the waveguide yields a mode confinement factor $\Gamma\approx1$. Finally, the calculated threshold gain is about 23.2 cm^{-1} shown in Fig. 2(b). From the threshold gain line, we can deduce the lasing domain (10.7→13.6 *kV/cm*).

We also calculated the lasing frequency with increasing bias which is shown in Fig. 3. The frequency in the lasing domain increases from 4.2 to 4.9 THz when the bias increases from 11 to 12.8 *kV/cm*. This spectral blueshift is due to the Stark shift of the intersubband gain curve versus applied electric field which is expected in the structures based on a nonintrawell transition [12].

The temperature evaluation of the device is carried out at the injection anticrossing bias and main results are shown in Fig. 4. In Figure 4(a), we plot the calculated current density *J* (left) and hot-phonon number (right) as a function of temperature. With the increase of temperature, the current density *J* is increasing monotonously. Similarly, by including the hot-phonon effect in our MC model, we find that the hot-phonon number shows a rapid increase from a few hundreds at lower temperatures to nearly 5×10^7 at 125 *K* on an arbitrary scale which indicates that LO-phonon emission is enhanced in a great degree with increasing temperature. Besides, the increase in hot-phonon number also reflects the importance of the hot-phonon effect in the simulations of carrier transport of the non-equilibrium devices, especially for high-temperature performance evaluation. The temperature dependent gain characteristics are shown in Fig. 4(b). The decreasing gain from 70 to 40 cm^{-1} with increasing temperature is clearly observed. Assuming the threshold gain for the device to be 23.2 cm^{-1}, the extrapolated maximum operating temperature is greatly higher than our measured value (90 *K*). The discrepancy between the simulation and the measurement is attributed to the exclusion of the

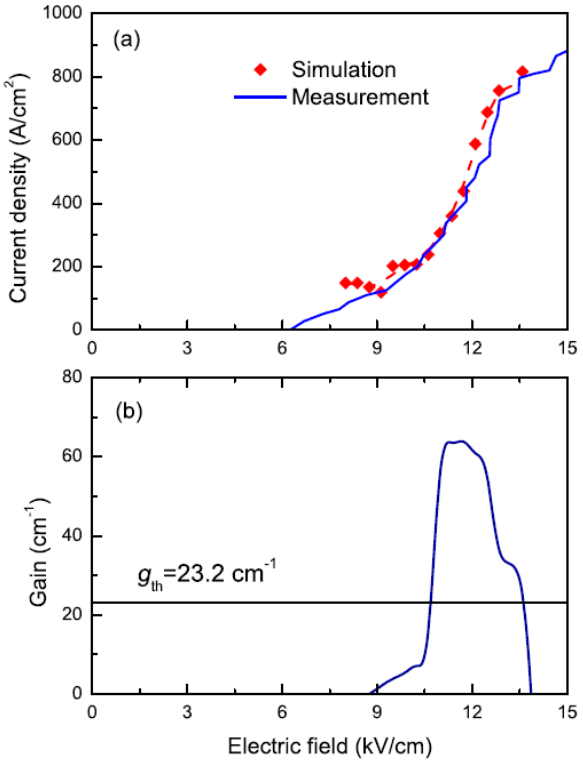

Fig. 2 (a) Calculated *I-V* characteristic of the device. The diamonds are sampling points and the dashed line provides a guide for the eye. As a reference, the measured curve is also indicated by a full line. (b) Material gain for a range of biases. The calculated threshold gain g_{th} is also indicated.

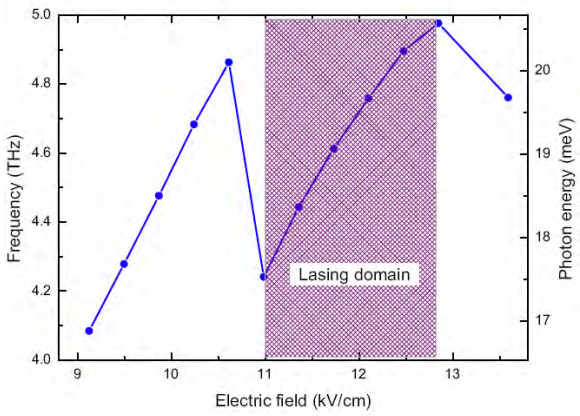

Fig. 3 Calculated lasing frequency of the THz QCL as a function of electric field.

broadening effect of temperature-dependent gain profile in our model. The increased broadening with increasing temperature will degrade the peak gain. The gain is proportional to $f_{54}\times\Delta N_{54}/\Delta v$ [11], here f_{54} is the oscillator strength, ΔN_{54} is the population inversion, and Δv is the full width of half maximum of the electroluminescence spectrum below threshold. In our calculations, we don't include the broadening effect and assume Δv to be a constant value

under all different temperatures. In fact, Δv, reflecting the broadening effect of gain profile, is increasing with temperature. Thereby, our calculations overestimate the gain and consequently overrate the maximum operating temperature. However, if we suppose Δv increase linearly from 2.6 *THz* at 25 *K* to 3.6 *THz* at 125 *K*, using an approximate formula $\Delta v=\tau_5^{-1}+\tau_4^{-1}$, another gain curve is obtained shown in Fig. 4(b) [lower curve]. Under the linear approximation condition, the maximum operating temperature is about 90 *K* which is consistent with the measurement.

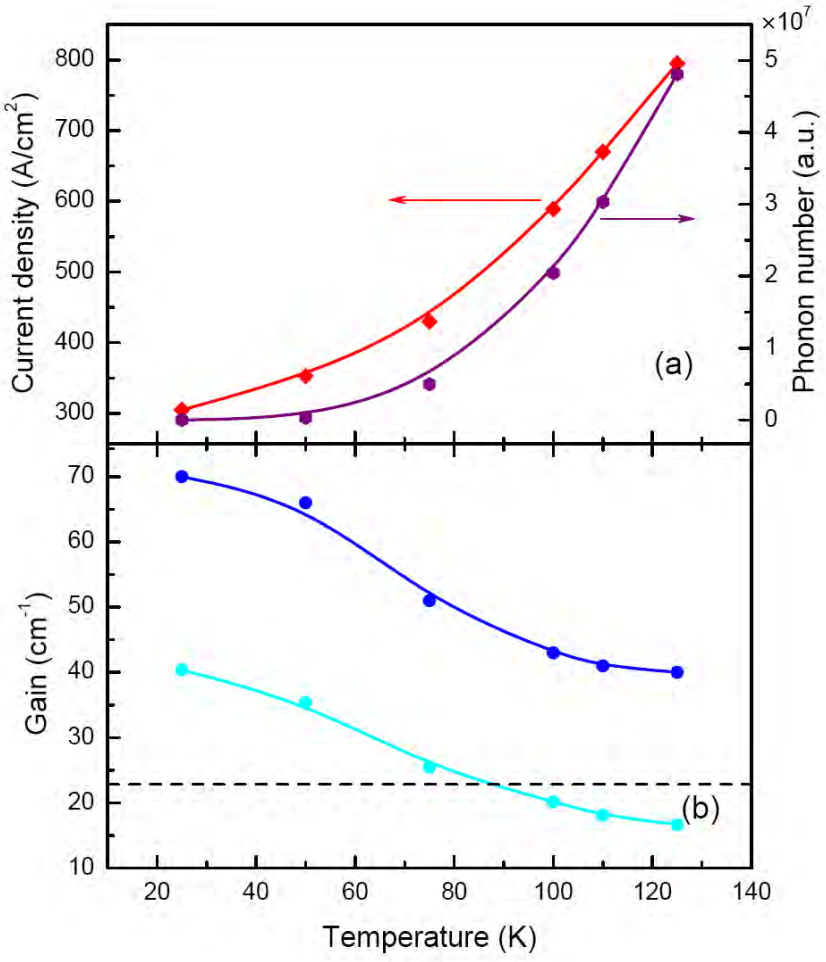

Fig. 4 (a) Calculated current density (left) and hot-phonon number (right) as a function of temperature. (b) Material gain with (lower) and without (upper) broadening effect for different temperatures. The threshold gain line is also indicated by a dashed line.

An investigation on the evolution of lasing frequency with temperature shows that the calculated lasing frequency is between 4.21 and 4.24 *THz* with the increase of temperature from 25 *K* to 125 *K*. The lasing frequency is mostly determined by the band structure, i.e., energy separation between lasing levels (E_{54}). In our MC simulation, the calculated E_{54} changes slightly which results in a relatively stable lasing frequency with increasing temperature. Compared with rigidly bias dependent lasing frequency, the frequency is more insensitive to temperature.

4. Conclusions

In conclusion, we have used an ensemble MC method, including e-e, e-p, e-i scatterings, and the hot-phonon effect, to evaluate the bias and temperature dependent performance of a 4.1 *THz* QCL. Carrier transport and gain characteristics are investigated. Due to the Stark effect, a blueshift of the emission spectra with increasing drive current is clearly observed. In the temperature evaluation of the device, we overestimate the peak gain and consequently overrate the maximum operating temperature because the temperature broadening of the gain profile is excluded in our MC model. Under a linear approximation condition, the deduced maximum operating temperature is in good agreement with experiment. The simulation also shows that the lasing frequency is insensitive to the temperature.

Acknowledgement

The authors are grateful to Professor H. C. Liu for useful discussions. This work is supported by the National Fund for Distinguished Young Scholars of China (60425415 and 60528005), the National Basic Research Program of China (2007CB310402), the National Natural Science Foundation of China (60721004 and 60606027), and the Shanghai Municipal Commission of Science and Technology (06dj14008, 06CA07001 and 07pj14103).

References

[1] R. Köhler, A. Tredicucci, F. Beltram, H. E. Beere, E. H. Linfield, A. G. Davies, D. A. Ritchie, R. C. Iotti and F. Rossi, "Terahertz semiconductor-heterostructure laser", *Natrue*, 417, 156-159, (2002).

[2] B. S. Williams, "Terahertz quantum-cascade lasers", *Nat. Photon.*, 1, 517-525, (2007).

[3] C. Walther, M. Fischer, G. Scalari, R. Terazzi, N. Hoyler and J. Faist, "Quantum cascade lasers operating from 1.2 to 1.6 THz", *Appl. Phys. Lett.*, 91, 131122, (2007).

[4] M. A. Belkin, J. A. Fan, S. Hormoz, F. Capasso, S. P. Khanna, M. Lachab, A. G. Davies and E. H. Linfield, "Terahertz quantum cascade lasers with copper metal-metal waveguides operating up to 178 K", *Opt. Express*, 16, 3242-3248, (2008).

[5] B. S. Williams, S. Kumar, Q. Hu and J. L. Reno, "Operation of terahertz quantum-cascade lasers at 164 K in pulsed mode and at 117 K in continuous wave mode", *Opt. Express*, 13, 3331-3339, (2005).

[6] B. S. Williams, S. Kumar, Q. Hu and J. L. Reno, "High-power terahertz quantum-cascade lasers", *Electron. Lett.*, 42, 89-90, (2006).

[7] C. Jacoboni and L. Reggiani, "The Monte Carlo method for the solution of charge transport in semiconductors with applications to covalent materials", *Rev. Mod. Phys.*, 55, 645-705, (1983).

[8] J. T. Lü and J. C. Cao, "Monte Carlo simulation of hot phonon effects in resonant-phonon-assisted terahertz quantum-cascade lasers", *Appl. Phys. Lett.*, 88, 061119, (2006).

[9] J. T. Lü and J. C. Cao, "Coulomb scattering in the Monte Carlo simulation of terahertz quantum-cascade lasers", *Appl. Phys. Lett.*, 89, 211115, (2006).

[10] H. Li, J. C. Cao and J. T. Lü, "Monte Carlo simulation of carrier transport and output characteristics of terahertz quantum cascade lasers", *J. Appl. Phys.*, 103, 103113, (2008).

[11] H. Li, J. C. Cao, J. T. Lü and Y. J. Han, "Monte Carlo simulation of extraction barrier width effects on terahertz quantum cascade lasers", *Appl. Phys. Lett.*, 92, 221105, (2008).

[12] B. S. Williams, H. Callebaut, S. Kumar, Q. H and J. L. Reno, "3.4-THz quantum cascade laser based on longitudinal-optical-phonon scattering for depopulation", *Appl. Phys. Lett.*, 82, 1015-1017, (2003).

[13] S. Kohen, B. S. Williams and Q. Hu, "Electromagnetic modeling of terahertz quantum cascade laser waveguides and resonators", *J. Appl. Phys.*, 97, 053106, (2005).

[14] M. A. Ordal, L. L. Long, R. J. Bell, S. E. Bell, R. R. Bell, R. W. Alexander, Jr and C. A. Ward, "Optical properties of the metals Al, Co, Cu, Au, Fe, Pb, Ni, Pd, Pt, Ag, Ti, and W in the infrared and far infrared", *Appl. Opt.*, 22, 1099-1119, (1983).